CrossMark

Ni deposited onto MWCNTs buckypapers for improved broadband EMI shielding

Yaoyao Bai[1] · Jijie Wang[1] · Shaowei Lu[2] · Zhenwei Huang[1] · Li Zhang[1] · Qiangang Xu[1] · Shifeng Xu[3]

Abstract

Highly flexible, mechanically robust and ultra-thin Ni deposited onto multi-walled carbon nanotubes (MWCNTs) bucky-papers (BPs) were fabricated via vacuum filtration and magnetron sputtering. The samples were characterized structurally using scanning electron microscopy and X-ray Diffraction. Electromagnetic interference (EMI) shielding effectiveness (SE) of Ni deposited onto MWCNTs BPs with different deposition time (0, 30 and 60 min) were tested in frequency range of 2–18 GHz, including S-band, C-band, X-band and Ku-band. The 60 min Ni deposited onto MWCNTs BPs exhibited much higher EMI SE of average value up to 42.59 dB with the thickness of only 0.105 mm. Based on reliability study, the 60 min Ni deposited onto MWCNTs BPs retains 94.3% of its EMI SE after 500 cycles of mechanical bending. Therefore, the results and techniques promise a simple and effective approach to achieve light-weight and ultra-thin composite films for a wide application at the prospect of the field of EMI shielding.

1 Introduction

The propagation of electronic gadgets and widespread instrumentation has generated electromagnetic interference (EMI) as radiation source [1]. Ranking together with noise, air and water pollution, EMI has been regarded as a novel public nuisance [2, 3]. In order to address this issue effectively, much attention has been paid to developing novel high-performance EMI shielding materials with a broadband frequency range [4–9]. The commercially used shielding materials included metal foil, metal laminates, metal screen and metal foam [10]. Nevertheless, as the most common EMI shields, metals usually have the problems of high density, poor corrosion resistance, and high processing costs [11]. However, in many applications (such as aerospace electronics), excepting being effective, the material for EMI shielding needs to be lightweight and flexible, especially in applications of flexible electronics, air-crafts and

automobiles. Since the density and flexibility of shielding materials are usually used for evaluate in EMI shielding applications, carbon material was used for competition with metals [12–16]. Since the initial development of the carbon nanotubes (CNT), its outstanding chemical and physical properties also resulted in excellent EMI properties [17]. More recently, CNTs shields with ultra-low density for EMI shielding have been reported. For example, with a citrate gel method, C.H. Phan et al. prepared multi-walled carbon nanotubes/manganese zinc ferrite hybrid fillers, the results show that composite exhibits excellent EMI shielding ability with the shielding effectiveness (SE) reaching average value of 44 dB at a thickness of 2 mm [18]. Gopal Kulkarni et al. reported that MWCNTs shows high shielding values varies from −65 to −45 dB at 8–12 GHz frequency range [19]. Yuan et al. demonstrated that the SWCNT/PANI composites resulted in EMI SE of 31.58 dB in the the range 2–18 GHz [20]. Liu and coworkers have reported multi-walled carbon nanotube, Fe and Fe_3O_4 epoxy composites exhibits excellent EMI SE up to 40 dB in the frequency range of 13–40 GHz [21]. Our team also made some works in EMI performance, we have reported that EMI shielding performance of single/multi-walled hybrid buckypaper composites, the results show that an average SE of ~55 dB with the thickness of 50 μm and density of 0.76 g cm^{-3} [22].

In this paper, we fabricated Ni deposited onto MWC-NTs buckypapers (BPs) via methods of vacuum filtration

✉ Shaowei Lu
  lushaowei_2005@163.com

1   Faculty of Materials Science and Engineering, Shenyang Aerospace University, Shenyang 110136, Liaoning, China

2   Faculty of Aerospace Engineering, Shenyang Aerospace University, Shenyang 110136, Liaoning, China

3   Faculty of Science, Shenyang Aerospace University, Shenyang 110136, Liaoning, China

and magnetron sputtering. The EMI shielding properties of Ni deposited onto MWCNTs BPs was investigated for the following reasons. Firstly, recent studies have shown that CNT possesses high real part (ϵ') of complex permittivity which represents the polarization. As a result, CNT has been explored for potential applications in EMI shielding [23–25]. Secondly, typical metals such as Ni, Ag and Cu are the most commonly used metallic fillers for EMI shielding. And in particular, Ni offers an appropriate choice owing to its lower cost than Ag and better thermal stability than Cu [26]. Finally, Ni as a magnetic metal is more attractive due to its high permeability, which is due to high saturation magnetization (Ms) and low coercivity (Hc) [27]. Therefore, by the combination of MWCNTs and Ni, the high EMI shielding of hybrid BPs can be obtained. This work provides an effective and convenient method to regulate EMI shielding in the broadband frequency range of 2–18 GHz, including S-band, C-band, X-band and Ku-band. Further, different frequency ranges have different applications. S-band is used in multimedia applications like mobile, TV, cordless phones, C-band is used in long distance radio communication, Wi-Fi devices, X-band is used in weather monitoring, air traffic control defence tracking and Ku-band is used in very small aperture terminal systems and so on [28].

2 Experimental

2.1 Materials preparation

MWCNTs with purity of higher than 95% was purchased from Chengdu Organic Chemicals Ltd, China Academy. The diameter and length of MWCNTs are in the range of 8–15 nm and 30–50 μm, respectively.

2.2 Sample preparation

2.2.1 Preparation of MWCNTs BPs

The MWCNTs BPs were fabricated by MWCNTs monodispersion via spry-vacuum filtration method. Each 500 mg MWCNTs and 5 ml Triton X-100 were added in 1000 ml distilled water to obtain MWCNTs aqueous solution. Then, the MWCNTs aqueous solution was sonicated (Q700, sonicator Co, Ltd, USA) for 3 times (each time 10 min) under 100 W. And after every sonication the MWCNTs solution was centrifuged for 30 min at a centrifuge speed of 6000 rpm/min. As shown in Fig. 1, the BPs were prepared by filtering the monodisperse solutions layer by layer through a 0.45 μm cellulose filter using a vacuum-pump. After the solution filtration, the samples were washed many times by distilled water to wash away the surfactant (Triton X-100) and dried at 80 °C for 12 h in air.
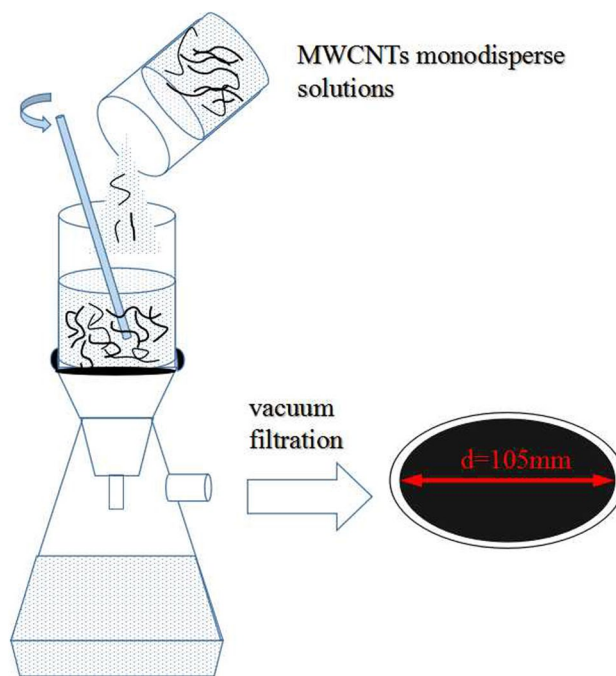

Fig. 1 Schematic illustration of the fabrication process of MWCNTs BPs

2.2.2 Fabrication of Ni deposited onto MWCNTs BPs

Ni deposited onto MWCNTs BPs were prepared by magnetron sputtering, which carried out in a pure argon atmosphere at a pressure of 0.3 Pa, as shown in Fig. 2 a. The target was a nickel plate (overall diameter, 50 mm). The MWCNTs BPs (Diameter: 105 mm) were placed parallel to the target surface as a substrate.

The prepared samples are labeled C_0, C_1 and C_2 corresponding to different deposition time of 0, 30 and 60 min, respectively, their properties are shown in Table 1.

2.3 Characterization

The surface morphology of pure MWCNTs BPs and Ni deposited onto MWCNTs BPs were characterized by scanning electron microscopy (SEM; NoVa Nano 15 kv). The Ni deposited onto MWCNTs BPs was characterized by using X-ray Diffraction (XRD) (Rigaku RINT2400 with Cu Kα radiation). A vibrating-sample magnetometer (VSM, Versalab) was used to study the magnetic properties of the Ni deposited onto MWCNTs BPs. The electrical conductivity of the samples was measured using a stand four-probe method. The average electrical conductivity and corresponding errors of each sample were determined by the three measured values.
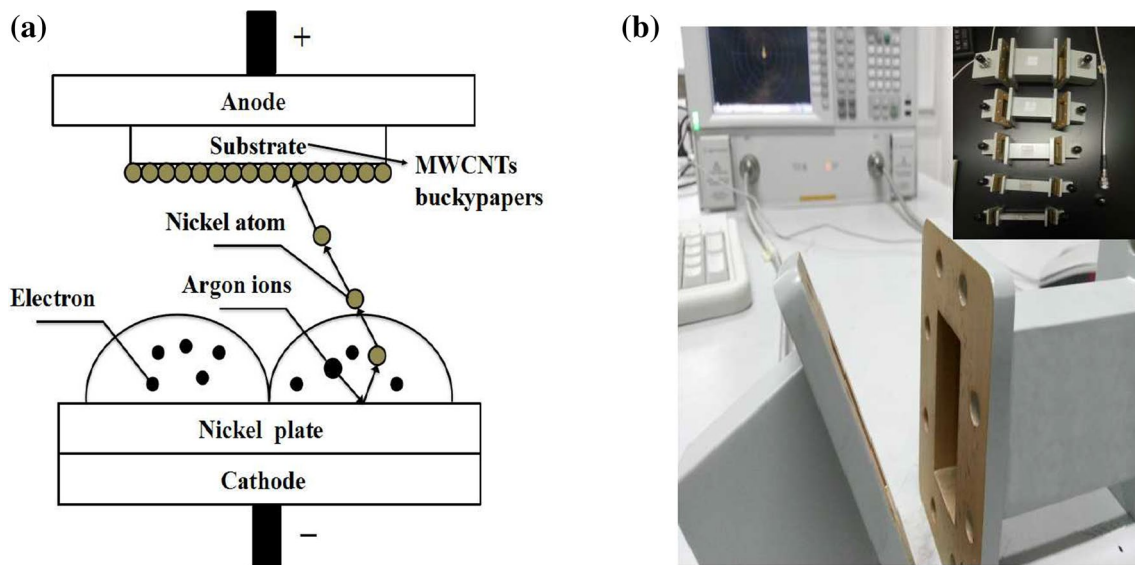
Fig. 2 Schematic illustration of Ni deposited onto MWCNTs BPs (**a**) the experiment setup for EMI shielding measurement (**b**)

Table 1 Basic properties of Ni deposited onto MWCNTs BPs

	Weight (mg)	Radius (mm)	Thickness (mm)	Deposition thickness (nm)	Deposition time (min)
C_0	538.3	105	0.103	0	0
C_1	526.2	105	0.095	~260	30
C_2	560.1	105	0.105	~480	60

2.4 EMI shielding

The S parameters (S_{11} and S_{21}) of the samples were measured by a two port Vector Network Analyzer (PAN-LN5230L Agilent Technologies) using the wave-guide method in the frequency range of 2–18 GHz, including S-band, C-band, X-band and Ku-band as shown in the upper right corner of Fig. 2 b. The dimension of sample holder is 72.14×34.04 mm for S-band, 47.59×22.15 mm for C-band, 22.86×10.16 mm for X-band and 15.79×7.89 mm for Ku-band, respectively. During the measurement, the film-like samples were sandwiched between the waveguide sample holders. The total SE (SET) as well as SE absorption (SEA) and SE reflection (SER) were determined based on the measured S parameters as follows:

$$R = |S_{11}|^2, \ T = |S_{21}|^2 \tag{1}$$

$$A = 1 - R - T \tag{2}$$

$$SER(dB) = -10\log(1 - R) \times SEA(dB) = -10\log(T/(1 - R)) \tag{3}$$

$$SET(dB) = 10\log\left(\frac{P_I}{P_T}\right) = SER + SEA \tag{4}$$

where R is reflection coefficient, T is absorption coefficient. P_I is the incident power, and P_T is the transmitted power.

3 Results and discussion

3.1 Microscopic observation

Figure 3 a shows the surface morphology of pure MWCNTs BPs. The pristine MWCNTs exhibits a strong tendency to form entanglement and agglomerate which was caused by the intermolecular van der waals force between MWCNTs. As shown in Fig. 3 b and c, it is clearly observed that Ni nanopowders are uniformly attached on the MWCNTs. The deposited Ni layer is more compact, as the deposition time increase from 30 to 60 min. At high magnification Fig. 3 d and e, the surface morphology of deposited Ni layer shows spherical nodular structure more clearly. This phenomenon is primarily attributed to the nanoscale protrusions and indentations on the MWCNTs surface-which act as nucleating sites for the Ni film. The nuclei grow isotropically, forming hemispherical nodules [29]. Moreover, it is observed that MWCNTs is visible after Ni deposited onto MWCNTs BPs. This is due to the three-dimensional network of MWCNTs
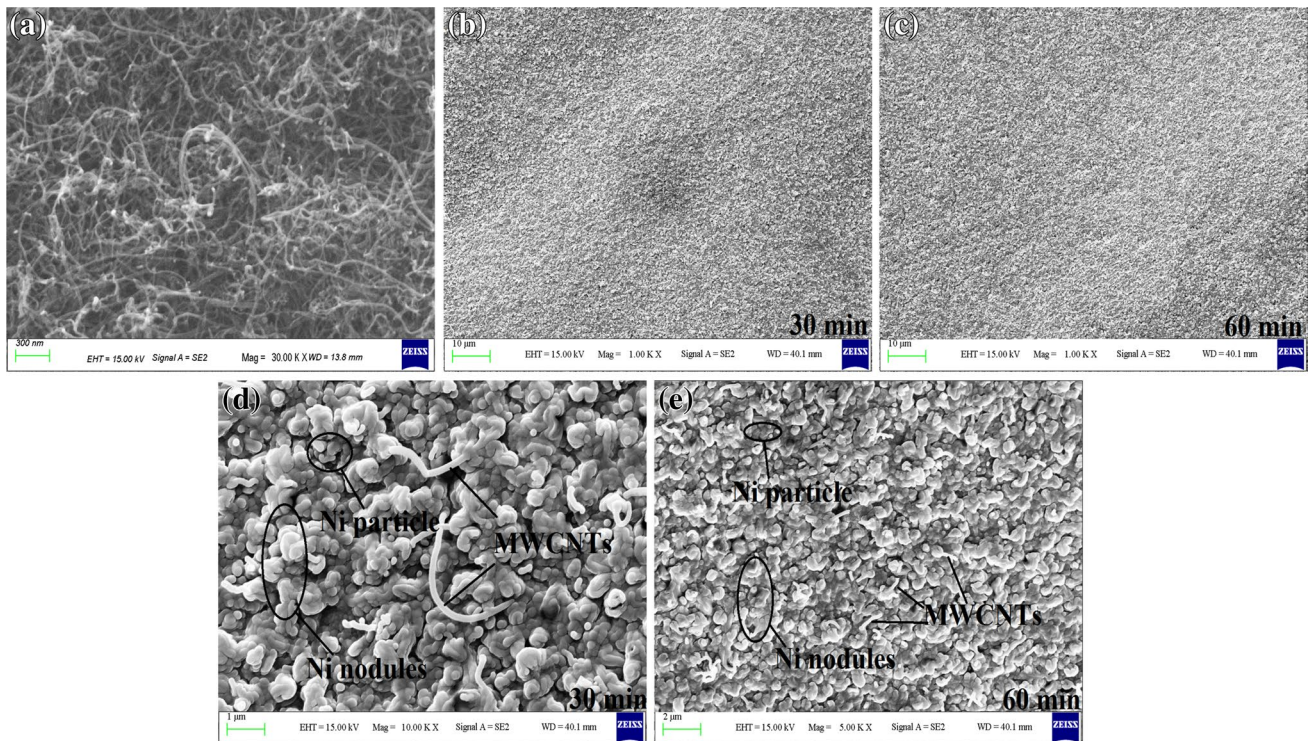
Fig. 3 Surface morphology of pure MWCNTs BPs (**a**) and Ni deposited onto MWCNTs BPs with different deposition time (**b–e**)
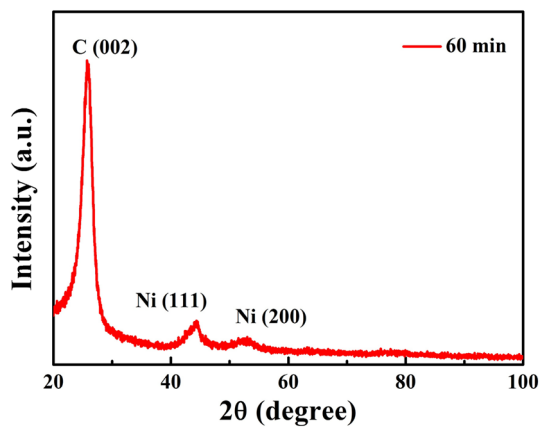

Fig. 4 XRD spectrum of the 60 min Ni deposited onto MWCNTs BPs

peak of the BPs at $2\theta = 26.1°$ are assigned to (002) plane of the graphite structure of MWCNTs. In addition, two peaks shown their presence at $2\theta = 44.5°$ and $51.2°$, which corresponded to Ni (111) and Ni (200) of faced-centered cubic (FCC) crystalline phase. The distinct peak at $44.5°$ appears, indicating the nucleation of Ni (111). During crystallization, Ni atoms naturally self-organize into FCC unit cells, whose highest planer density occur on the (111) facts. As observed, the presence of Ni (111) and Ni (200) facets indicates Ni is present on the surface of MWCNTs BPs with the crystallization.

3.3 Magnetic properties

The magnetic hystersis curves of 60 min Ni deposited onto MWCNTs BPs at room temperature are shown in Fig. 5. It can be seen that 60 min Ni deposited onto MWCNTs BPs has the obvious hysteresis loop. The value of saturation Ms of 60 min Ni deposited onto MWCNTs BPs is 9.61 emu/g and Hc is 85.16 Oe. Because the deposition thickness of Ni is limited of several 100 nm, the Ms and Hc are not high. But it can still be attracted by magnets. Theoretically, the shielding materials with magnetic properties will exhibit relatively high EMI SE [30].
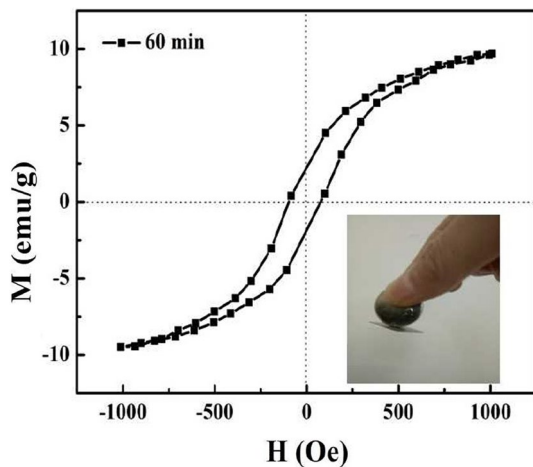
BPs. Ni are surrounded by the strong intermolecular van der waals force between MWCNTs. As a result, Ni deposited onto MWCNTs BPs has excellent mechanical robustness and good flexibility.

3.2 XRD analysis

Figure 4 shows the XRD spectra of the 60 min Ni deposited onto MWCNTs BPs. It is observed that the diffraction

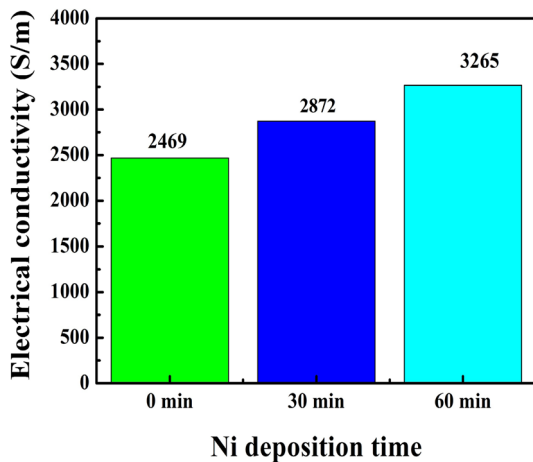**Fig. 5** The magnetic hysteresis loops of 60 min Ni deposited onto MWCNTs BPs

Fig. 6 The electrical conductivity of BPs

3.4 Conductivity measurements

The electrical conductivity of shielding materials has an intimate connection with their EMI shielding performance [11, 31]. The results of the average conductivity for BPs demonstrate that the conductivity increases from 2469 to 3265 S/m as the Ni deposition time increases from 0 to 60 min, shown in Fig. 6. This phenomenon is the direct result of the increased amount of deposited Ni onto the MWCNTs surface with increasing deposition time. Ni has a higher electrical conductivity than carbons, this leads to a faster drift velocity for the electrons in the Ni film compared to MWCNTs [32, 33]. Therefore, a more effective conductive pathway is formed through Ni layer in addition to the original electrical conductive MWCNTs network.

3.5 EMI shielding performance

Figure 7 a shows the SET of MWCNTs BPs with different Ni deposition times tested in the frequency range of 2–18 GHz. Compared with SET value of 22–31 dB of pure MWCNTs BPs, the SET value of Ni deposited onto MWCNTs BPs has been increased significantly, the SET of 30 min Ni deposited onto MWCNTs BPs reach to 34–42 dB, the SET of 60 min Ni onto deposited MWC-NTs BPs reach to 39–47 dB. Based on general requirement of commercial EMI shielding application (20 dB) [34], MWCNTs BPs with or without deposited Ni layer all qualified as effective EMI shielding materials. The above results have suggested that the deposition of Ni could improve the final EMI shielding performance of MWCNTs BPs.

To further clarify the underlying mechanism, the direct comparison of SEA and SER between MWCNTs BPs with different Ni deposition time was also investigated, as shown in Fig. 7 b and c. And the average value of SET, SEA and SER were all shown in Fig. 7 d. It is obvious that the SEA rises noticeably with the increase of deposition time, while the value of SER has not changed much, which means that contribution of the SEA to the SET dominates that of the SER. For instance, the average SET, SEA and SER of 60 min Ni deposited onto MWCNTs BPs were 42.59, 32.01 and 10.58 dB, respectively in Fig. 7 d. The contribution of SEA (75.16%) was higher than that of SER (24.84%), which suggested the SEA was main shielding mechanism. According to EMI shielding mechanisms, SEA steams mainly from dielectric loss and magnetic loss [35]. On one hand, the dielectric loss involves relaxation and conduction loss, which are respectively influenced by polarization and conductivity [36]. Futhermore, the polarization derives from defects, interfaces and functional groups [37–39]. The high conductivity of the Ni deposited onto MWCNTs BPs contributes a lot to the conduction loss, as well as interface between Ni and MWCNTs together with the crystal defects can also induce the polarization and contribute to relaxation loss [40–44]. On the other hand, the magnetic loss was mainly influenced by the magnetic properties. The Ni deposited onto MWCNTs BPs with magnetic properties contributes a lot to the magnetic loss. With the effect of the above aspects, the 60 min Ni deposited onto MWCNTs shows a higher shielding efficiency.

For 60 min Ni deposited onto MWCNTs BPs, deposited Ni confers its high EMI shielding performance. To ensure its stability under mechanical deformation, it was validated by its SET measurement before and after 500 times repeated bending. As shown in Fig. 8, it is observed that the SET of the Ni deposited onto MWCNTs BPs shows a very small decrease after repeatedly bending 500 times. The average SET of Ni deposited onto MWCNTs BPs is 40.15 dB
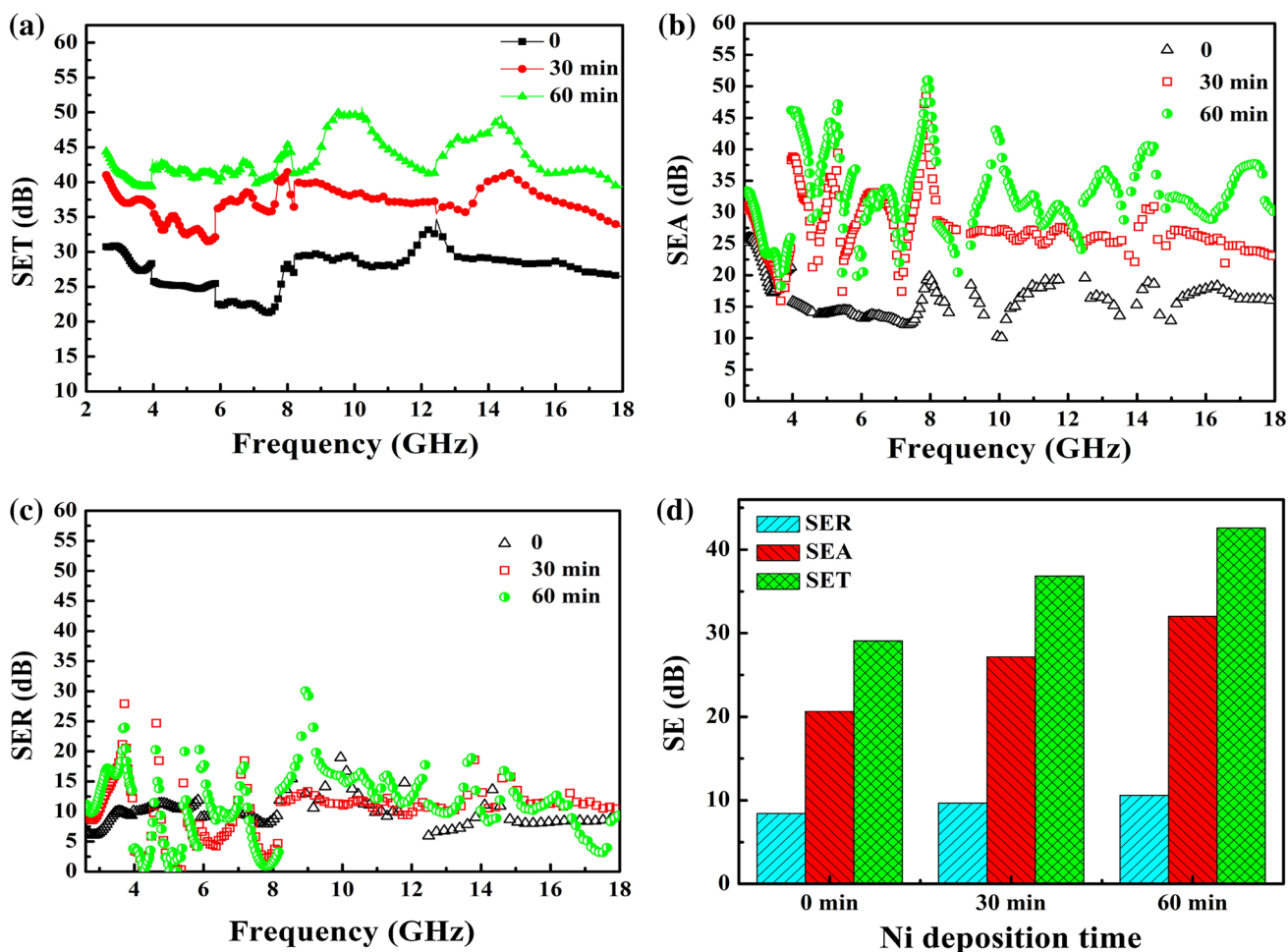
Fig. 7 SET, SEA and SER of BPs in the frequency range of 2–18 GHz (**a–c**), the average SEA, SER and SET of BPs in the freguency range of 2–18 GHz (**d**)
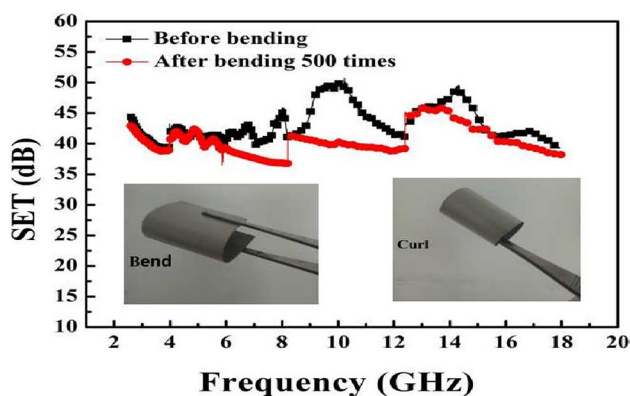

Fig. 8 SET of 60 min Ni-deposited MWCNTs BPs before and after bending to a radius of 2.5 mm repeatedly for 500 times

after bending 500 cycles. After being mechanically bending for 500 times, Ni deposited onto MWCNTs BPs retains 94.3% of its EMI SE performance. This experimental result

indicates that Ni deposited onto MWCNTs BPs has excellent mechanical robustness and good flexibility.

Table 2 makes a comparison of the SET of various material reported in the literature [20, 45–50], from which we can see clearly that carbon-based materials generally exhibited far more advantages, in fabricating ultra-thin EMI shields. Through directly comparing the total SE values, and the result demonstrated that 60 min Ni deposited onto MWCNTs BPs shows higher shielding efficiency and wider bandwidth than other materials with much larger sample thickness.

4 Conclusion

In summary, ultra-thin, flexible, and lightweight Ni deposited onto MWCNTs BPs were fabricated by vacuum filtration and magnetron sputtering. The Ni deposited onto MWCNTs BPs in terms of EMI shielding efficiency was investigated in a broadband frequency range of 2–18 GHz,

Table 2 Comparison of the recently reported materials and their corresponding performance

	Thickness (mm)	SET (dB)	Shield frequency (GHz)	Reference
Graphene/polymer	0.35	27	8–12	[45]
MWCNT/rGO	2.4	37	12.4–18	[46]
CNT/PDMS	2	46.3	8–12	[47]
PANI/graphene	0.05	32	8–12	[48]
PU/graphene	2	32	8–12	[49]
SWCNT/PANI	2.4	31.5	2–18	[20]
G-foam	0.3	25.2	8–12	[50]
Ni/MWCNTs	0.105	42.59	2–18	This work

including S-band, C-band, X-band and Ku-band. The results show that the 60 min Ni deposited onto MWCNTs BPs exhibited much higher EMI SE of average value up to 42.59 dB, with the thickness of 0.105 mm that is higher than other previous thickness materials. In addition, the Ni deposited onto MWCNTs BPs exhibited the mechanical stability. After being mechanically bent for 500 cycles, the Ni deposited onto MWCNTs BPs shows a very small decrease of its SET, demonstrating a good mechanical robustness.

References

1. S. Bi et al., Comparative study of electroless Co-Ni-P plating on Tencel fabric by Co 00-based and Ni 00-based activation for electromagnetic interference shielding. Appl. Surf. Sci. **419**, 465–475 (2017)
2. S.C. Lin et al., Electromagnetic interference shielding performance of waterborne polyurethane composites filled with silver nanoparticles deposited on functionalized graphene. Appl. Surf. Sci. **385**, 436–444 (2016)
3. H. Liu et al., Preparation and the electromagnetic interference shielding in the X-band of carbon foams with Ni-Zn ferrite additive. J. Eur. Ceram. Soc. **36**(16), 3939–3946 (2016)
4. B. Shen et al., Strong flexible polymer/graphene composite films with 3D saw-tooth folding for enhanced and tunable electromagnetic shielding. Carbon **113**, 55–62 (2016)
5. B. Shen, W. Zhai, W. Zheng, Ultrathin flexible graphene film: an excellent thermal conducting material with efficient emi shielding. Adv. Funct. Mater. **24**(28), 4542–4548 (2014)
6. B. Wen et al., Reduced graphene oxides: light-weight and high-efficiency electromagnetic interference shielding at elevated temperatures. Adv. Mater. **26**(21), 3484–3489 (2014)
7. Y. Chen et al., High-performance epoxy nanocomposites reinforced with three-dimensional carbon nanotube sponge for electromagnetic interference shielding. Adv. Funct. Mater. **26**(3), 447–455 (2016)
8. Y. Zhang et al., Broadband and tunable high-performance microwave absorption of an ultralight and highly compressible graphene foam. Adv. Mater. **27**(12), 2049 (2015)
9. H. Sun et al., Cross-stacking aligned carbon-nanotube films to tune microwave absorption frequencies and increase absorption intensities. Adv. Mater. **26**(48), 8120–8125 (2014)
10. L. Wang et al., Influence of metal screen materials on 3-D electromagnetic field and eddy current loss in the end region of turbogenerator. IEEE Trans. Magn. **49**(2), 939–945 (2013)
11. Y. Li et al., Ultrathin carbon foams for effective electromagnetic interference shielding. Carbon **100**, 375–385 (2016)
12. L. Zhang et al., Preparation and characterization of graphene paper for electromagnetic interference shielding. Carbon **82**(30), 353–359 (2015)
13. Z. Chen et al., Lightweight and flexible graphene foam composites for high-performance electromagnetic interference shielding. Adv. Mater. **25**(9), 1296–1300 (2013)
14. A. Fletcher et al., Elastomer foam nanocomposites for electromagnetic dissipation and shielding applications. Compos. Sci. Technol. **70**(6), 953–958 (2010)
15. H.B. Zhang et al., Tough graphene-polymer microcellular foams for electromagnetic interference shielding. ACS Appl. Mater. Interfaces **3**(3), 918 (2011)
16. Y. Yang et al., Novel carbon nanotube-polystyrene foam composites for electromagnetic interference shielding. Nano Lett. **5**(11), 2131–2134 (2005)
17. H.H. Zhao et al., Electrophoretic deposition of foam Ni/CNT composites and their electromagnetic interference shielding performance. Appl. Mech. Mater. **461**, 436–444 (2013)
18. C.H. Phan, M. Mariatti, Y.H. Koh, Electromagnetic interference shielding performance of epoxy composites filled with multi-walled carbon nanotubes/manganese zinc ferrite hybrid fillers. J. Magn. Magn. Mater. **401**, 472–478 (2016)
19. G. Kulkarni et al., Enhanced electromagnetic interference shielding effectiveness of chemical vapor deposited MWCNTs in X-band region. J. Mater. Sci.: Mater. Electron. **28**(10), 7212–7220 (2017)
20. B. Yuan et al., Comparison of electromagnetic interference shielding properties between single-wall carbon nanotube and graphene sheet/polyaniline composites. J. Phys. D **45**(23), 235108 (2012)
21. Y. Liu et al., EMI shielding performance of nanocomposites with MWCNTs, nanosized Fe 3 O 4 and Fe. Compos. B Eng. **63**(7), 34–40 (2014)
22. S. Lu et al., Fabrication of single/multi-walled hybrid buckypaper composites and their enhancement of electromagnetic interference shielding performance. J. Phys. D **49**(44), 445308 (2016)
23. L.L. Wang et al., Electromagnetic interference shielding effectiveness of carbon-based materials prepared by screen printing. Carbon **47**(8), 1905–1910 (2009)
24. Y. Li et al., Electrical conductivity and electromagnetic interference shielding characteristics of multiwalled carbon nanotube filled polyacrylate composite films. Appl. Surf. Sci. **254**(18), 5766–5771 (2008)
25. W.-L. Song et al., Synthesis of zinc oxide particles coated multiwalled carbon nanotubes: dielectric properties, electromagnetic interference shielding and microwave absorption. Mater. Res. Bull. **47**(7), 1747–1754 (2012)
26. C.F. Goh et al., The effect of annealing on the morphologies and conductivities of sub-micrometer sized nickel particles used for

electrically conductive adhesive. Thin Solid Films **504**(1), 416–420 (2006)

27. D.-X. Yan et al., Efficient electromagnetic interference shielding of lightweight graphene/polystyrene composite. J. Mater. Chem. **22**(36), 18772 (2012)

28. A. Joshi, S. Datar, Carbon nanostructure composite for electromagnetic interference shielding. Pramana **84**(6), 1099–1116 (2015)

29. M. Sano et al., Application of supercritical carbon dioxide in catalyzation and Ni-P electroless plating of nylon 6,6 textile. Surf. Coat. Technol. **302**, 336–343 (2016)

30. R. Wang et al., Preparation and characterization of a kind of magnetic carbon fibers used as electromagnetic shielding materials. J. Alloys Compd. **514**(5), 35–39 (2012)

31. D.D.L. Chung, Carbon materials for structural self-sensing, electromagnetic shielding and thermal interfacing. Carbon **50**(9), 3342–3353 (2012)

32. J.N. Balaraju et al., Studies on electroless nickel polyalloy coatings over carbon fibers/CFRP composites. Surf. Coat. Technol. **302**, 389–397 (2016)

33. S.S. Tzeng, F.Y. Chang, Electrical resistivity of electroless nickel coated carbon fibers. Thin Solid Films **388**(1), 143–149 (2001)

34. Y. Wang et al., Reduced graphene oxide (RGO)/Mn3O4 nanocomposites for dielectric loss properties and electromagnetic interference shielding effectiveness at high frequency. Ceram. Int. **42**(1), 936–942 (2016)

35. H. Mei et al., Improvement of the electromagnetic shielding properties of C/SiC composites by electrophoretic deposition of carbon nanotube on carbon fibers. Carbon **109**, 149–153 (2016)

36. M. Arjmand et al., Effect of synthesis catalyst on structure of nitrogen-doped carbon nanotubes and electrical conductivity and electromagnetic interference shielding of their polymeric nanocomposites. Carbon **98**, 358–372 (2016)

37. B. Wen et al., Reduced graphene oxides: the thinnest and most lightweight materials with highly efficient microwave attenuation performances of the carbon world. Nanoscale **6**(11), 5754–5761 (2014)

38. W.Q. Cao et al., Temperature dependent microwave absorption of ultrathin graphene composites. J. Mater. Chem. C **3**(38), 10017–10022 (2015)

39. F. Sharif et al., Segregated hybrid poly (methyl methacrylate)/graphene/magnetite nanocomposites for electromagnetic interference shielding. ACS Appl. Mater. Interfaces **9**(16), 14171–14179 (2017)

40. M. Zong et al., Facile preparation, high microwave absorption and microwave absorbing mechanism of RGO–Fe3O4 composites. RSC Adv. **3**(45), 23638–23648 (2013)

41. D. Chen et al., Controllable fabrication of mono-dispersed RGO-hematite nanocomposites and their enhanced wave absorption properties. J. Mater. Chem. A **1**(19), 5996–6003 (2013)

42. Y. Zhai et al., Enhanced microwave absorbing performance of hydrogenated acrylonitrile–butadiene rubber/multi-walled carbon nanotube composites by in situ prepared rare earth acrylates. Compos. Sci. Technol. **72**(6), 696–701 (2012)

43. X.F. Zhang, J.J. Guo, G.W. Qin, Assembled micro-nano particles with multiple interface polarizations for electromagnetic absorption at gigahertz. Appl. Phys. Lett. **104**(25), 8392 (2014)

44. B. Wen et al., Temperature dependent microwave attenuation behavior for carbon-nanotube/silica composites. Carbon **65**(12), 124–139 (2013)

45. W.-L. Song et al., Flexible graphene/polymer composite films in sandwich structures for effective electromagnetic interference shielding. Carbon **66**, 67–76 (2014)

46. A.P. Singh et al., Probing the engineered sandwich network of vertically aligned carbon nanotube–reduced graphene oxide composites for high performance electromagnetic interference shielding applications. Carbon **85**, 79–88 (2015)

47. D. Lu et al., Flexible, lightweight carbon nanotube sponges and composites for high-performance electromagnetic interference shielding. Carbon **133**, 457–463 (2018)

48. R. Mohan et al., Polyaniline/graphene hybrid film as an effective broadband electromagnetic shield. RSC Advances **5**(8), 5917–5923 (2015)

49. S.T. Hsiao et al., Using a non-covalent modification to prepare a high electromagnetic interference shielding performance graphene nanosheet/water-borne polyurethane composite. Carbon **60**(14), 57–66 (2013)

50. B. Shen et al., Microcellular graphene foam for improved broadband electromagnetic interference shielding. Carbon **102**, 154–160 (2016)